SSC20-XI-01

A GaN-based Four-Switch Buck-Boost Converter using Ripple Correlation Control for Maximum Power Point Tracking in Dynamic Deep Space Environments

Sadab Mahmud, William Collings, Roshan Kini, Ahmad Javaid, Raghav Khanna
University of Toledo
2801 West Bancroft Street, Toledo, OH 43606; (419)5308183
sadab.mahmud@utoledo.edu

Ansel Barchowsky, Jessica Loveland, Ahmadreza Amirahmadi, Chris Stell
Jet Propulsion Laboratory, California Institute of Technology
4800 Oak Grove Drive, Pasadena, CA 91109
ansel.barchowsky@jpl.nasa.gov

Xavier Zapien
Massachusetts Institute of Technology
77 Massachusetts Ave, Cambridge, MA 02139
xzapien@mit.edu

ABSTRACT

As the demand for high-performance power conversion in spacecraft continues to grow and spacecraft mass and volume budgets become increasingly tight, it is essential to design DC-DC converters with higher efficiency and power density. Although photovoltaic (PV) efficiency has increased over time, solar irradiance and temperatures can fluctuate dramatically in deep space. This causes significant variations in the maximum power point (MPP) of the PV array, which can decrease the overall system efficiency unless accounted for. Thus, it is imperative to track the MPP of the PV panels to maintain optimal efficiency. This paper presents the experimental development of a four-switch, GaN-based buck-boost converter with an implementation of the Ripple Correlation Control (RCC) MPPT algorithm for dynamic deep space environments. Due to the use of GaN HEMTs, the experimental system achieves better efficiency and power density compared to the previous state of the art implementations. A simulation of the prototype buck-boost converter was implemented in SaberRD (Synopsis), and a digital design of the RCC-based MPPT controller utilizing the StateAMS tool is presented. The simulation results show that this controller swiftly and precisely converged to the MPP of the source PV panels in a dynamic solar irradiance condition.

I. INTRODUCTION

Among the limited options to power a spacecraft, solar energy is a major contributor. PV panels are now more efficient with new materials utilizing multi-junction cells to capture more energy from the solar spectrum [1], [2]. However, the fact that there are changes in the nonlinear output characteristics curve with variations in solar insolation and temperature [3] establishes the need for power converters employed using maximum power point tracking (MPPT). Designing high performance power converters with MPPT becomes more necessary since aerospace system demands for computation and instrumentation needs are ever increasing [4], [5].

Solar array irradiance can drop significantly during deep space missions, thereby hindering system performance. In addition, compared to terrestrial PV systems, spacecraft PV systems will experience a profound change in solar insolation and temperature. Fig. 1 demonstrates this by representing data collected during NASA's Soil Moisture Active Passive (SMAP) mission. From Fig. 1, the volatile temperature swings during one orbital cycle and the rapid change in MPP of the solar cell over the same time can be seen. To obtain maximum efficiency during these dynamic conditions, the controller for the DC-DC converter must have MPPT capabilities.

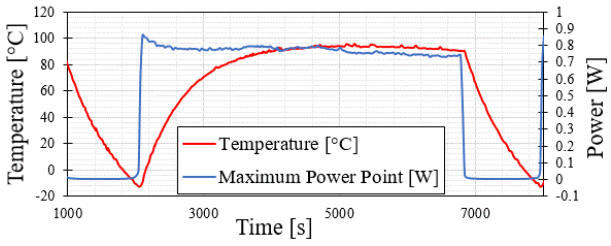

Figure 1: Change in solar cell temperature and maximum power point through orbital cycle.

One of the major focuses for space-oriented PV systems is small size and portability since there are mass and volume constraints placed upon these systems. Therefore, along with MPPT control improvement, physical optimization must also be included [6], [7] leading to the need for power delivery circuits with high power density. Wide bandgap (WBG) semiconductors such as gallium nitride (GaN) and silicon carbide (SiC) devices are the lead runners for next generation power electronic circuits. In order to achieve a high efficiency and power density in power converter circuits, GaN devices play an essential role. Compared to traditional flight qualified silicon (Si) devices, GaN has a high electron mobility which allows it to operate efficiently in high frequency applications [8], [9]. Studies have also shown GaN to be radiation hardened and suitable for space environments [10]. By using a high frequency to operate the power converter, the physical size of the inductors and capacitors in the DC-DC converter can be greatly reduced. With reduced passive component size coupled with the good high-frequency performance of GaN devices, a DC-DC converter board with high power density can be realized.

As previously highlighted, an MPPT controller for power converters in space is a necessity. The Ripple Correlation Control (RCC) [11-15] is a suitable MPPT method which can accurately track the MPP of the PV array in dynamic solar irradiation conditions. RCC utilizes the ripples inherent to the power converter due to its switching activity. By correlating the inherent PV array power ripples and the inductor current ripples of the DC-DC converter, the RCC method can drive the PV array to its MPP and does not need any sort of external perturbation [11]. The RCC technique has been shown to be well developed and suited to work digitally with microcontrollers as well [14], [15]. A digital controller will be helpful to avoid multiple analog ICs and hence reduce the number of components further aiding to a high power density design.

This paper presents the design and development of a GaN-based four-switch buck-boost converter which has experimentally achieved higher efficiency compared to the previous state of the art power converter implementations. This prototype converter achieved an improved efficiency of greater than 95%. A simulation of this converter was implemented in SaberRD (Synopsis) and the RCC-based MPPT controller model for it was developed using the built-in StateAMS tool in SaberRD. The controller demonstrated the RCC functionality by accurately and dynamically tracking the MPP of the input PV array. The controller design logic implemented here can be ported to any microcontroller to be used as a digital RCC controller for any power converter application.

This paper begins with a review of RCC in section II. The development and specifics of the prototype buck-boost converter is shown in section III. Section IV details the simulation of the prototype board along with the design of the digital RCC-based MPPT controller. This section also proves the efficacy of the controller in dynamic solar irradiance conditions. The paper is concluded, and future work is discussed in section V.

II. RIPPLE CORRELATION CONTROL

In a wide range of MPPT techniques, RCC is among the few which supports an analog implementation [11] and it is also presented in a digital form in [14], [15]. The principle and formulation of RCC is well established and discussed in [11]. Fig. 2 shows a generic PV output characteristic curve with average PV power on the y-axis vs. the average inductor current on the x-axis.

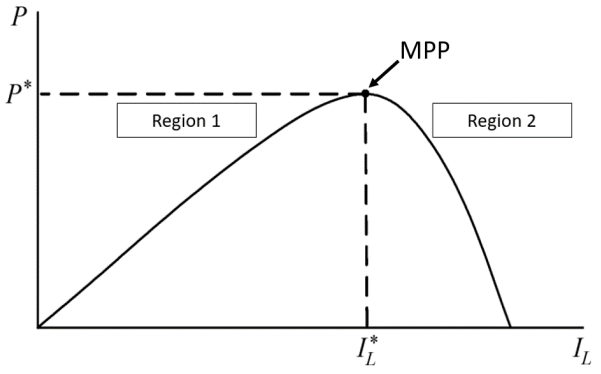

Figure 2: PV array average power versus average inductor current. [11]

The curve in Fig. 2 indicates that the derivative of the power, P, with respect to the inductor current, I_L, is positive to the left of MPP marked as region 1, negative to the right of MPP marked as region 2, and zero at the MPP. By inspecting Fig. 2, it is observed that in region 1, the current ripple imposed here leads to an in-phase power ripple since an increase in I_L results in an increase in P. Conversely, in region 2, the current ripples and power ripples are separated by 180°, or in other words, they are out-of-phase. The RCC principle is based on this relation between the relative phase of the current and power perturbation and it is necessary for the RCC algorithm to work. These observations can be combined as follows [11]:

$$\frac{di_L}{dt}\frac{dP}{dt} > 0 \rightarrow \text{Region 1} \quad (1)$$

$$\frac{di_L}{dt}\frac{dP}{dt} < 0 \rightarrow \text{Region 2} \quad (2)$$

Furthermore, the input current and the inductor current of the power converter are dependent on the duty ratio. This makes it possible to traverse the power curve shown in Fig. 2 by changing the duty cycle of the power converter. Therefore, (1) and (2) can be combined to generate a duty ratio, *d* in the form of an integral control law with a suitable scalar gain, *k* as [11]:

$$d = k \int \frac{di_L}{dt} \frac{dP}{dt} dt \quad (3)$$

A variation of (3) can be formulated by using the signum or sign function applied to the derivatives to obtain absolute values. By using this, it becomes easier to implement since the sign function clips the noise caused by differentiation. The sign function is shown in (4) and the modified RCC control law in (5) [11].

$$sign(x) = \begin{cases} 1; x > 0 \\ 0; x = 0 \\ -1; x < 0 \end{cases} \quad (4)$$

$$d = k \int sign\left(\frac{di_L}{dt}\right) sign\left(\frac{dP}{dt}\right) dt \quad (5)$$

The RCC control law in (5) is particularly useful for implementation in the digital domain using micro-controllers. This paper leverages this control law in the development of the RCC-based digital controller in SaberRD. By correlating the sign information of the time-based derivatives of the panel power and inductor current, the changes in the duty cycle of the converter can be determined which eventually stabilizes to a value reflecting the MPP of the panel.

Overall, RCC is a well-established algorithm which can achieve MPP at a fast-tracking rate in rapidly changing atmospheric conditions and solar irradiance. It is in principle an enhanced version of the traditional "perturb & observe" (P&O) algorithm [16] with the exception that RCC does not require an external perturbation source and that it tracks the MPP more precisely. Also, RCC does not rely on any assumptions or characterization of the PV array, it is an array independent algorithm and the RCC-based controller can be interfaced with any variety of PV based power source.

III. BUCK BOOST CONVERTER PROTOTYPE

To accommodate the wide fluctuations in array voltage observed throughout the course of a mission, a four-switch synchronous buck-boost converter was implemented, using commercially available GaN transistors [17], to achieve performance improvement over flight-qualified Si MOSFETs. Unlike the traditional single switch buck-boost converter, the synchronous buck-boost converter produces a non-inverting output, which facilitates integration with the spacecraft load power rails. Compared to other converter topologies, this synchronous converter can usually achieve higher power conversion efficiency because of its low voltage and current stress [18]. It is operated by providing coordinated gating signals to the four switches. Due to this coordinated switching activity, the overall voltage and current stress in the converter is lowered [18]. The prototype board is shown in Fig. 3.

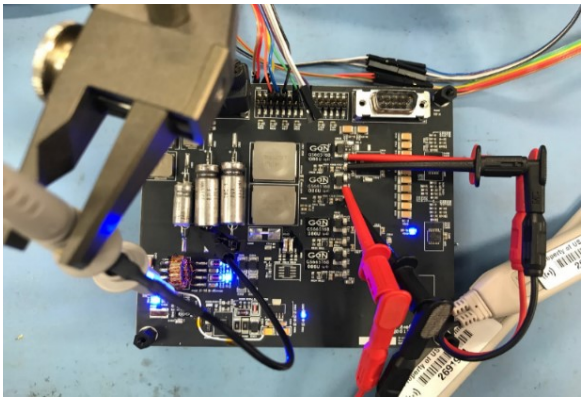

Figure 3: Prototype buck-boost solar array converter in testing.

The total ionizing dose (TID) and single event effects (SEE) [4], are commonly observed phenomena in deep space. The total amount of radiation that an electronic component is exposed to is referred to as the TID [4]. SEE, on the other hand is caused by heavily charged particles that penetrate sensitive nodes and results with ICs abruptly malfunctioning [4]. Several studies have been performed on the radiation effects on GaN devices. As like any semiconductor device, results found in [19] reveal that, under heavy radiation there can be adverse effects on a GaN transistor which can alter its V_{DS} or V_{GD} and rupture the dielectric layer. Proper immunity to TID and SEE can only be achieved by semiconductor devices with additional shielding, but the findings in [10] conclude that GaN devices can function in space environments with minimal shielding and might even operate safely without any shielding for several years. According to the studies performed in [20] and [21], the GaN HEMTs utilized in this design have been demonstrated to be hardened to both TID and SEE. Furthermore, compared to radiation hardened Si MOSFETs, the GaN device used in this prototype has a better trade-off between on-resistance and device capacitance as shown in Fig. 4.

The converter parameters are shown in Table 1. An auxiliary fly-back converter was used for local derivation of housekeeping supplies and to allow for full duty-cycle operation of the power stage. This capability enables the converter to operate closely to direct energy

transfer (DET) where the maximum power point follows the bus voltage. Such string switching techniques for efficient power regulation on spacecraft were also presented in [22].

Table 1: Operational Parameters for the Prototype Buck-boost Converter

Parameter	Design Value
Input Voltage	20 – 100V
Output Voltage	22 – 36 V
Processing Power	100 W
Switching Frequency	1 MHz
GaN Device	GS66516B

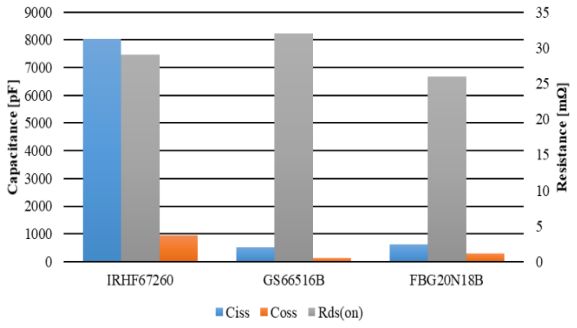

Figure 4: Comparison of critical device parameters for radiation hardened Si MOSFETs and GaN HEMTs. [23]

As established earlier, a major requirement for power converters in space applications is having a higher power density. Since the physical size of the passive components in a DC-DC converter is inversely proportional to the switching frequency of the converter, it becomes necessary to operate the power converter at a high switching frequency [24]. WBG semiconductors, especially GaN, have developed a reputation of functioning at high frequencies with minimal loss. Studies performed in [25] and [26] have shown that, at higher switching frequencies, GaN achieved superior efficiency when compared to its similarly specified Si counterpart.

After testing this prototype board, it was found that this system achieved an improved specific power greater than 1 kW/kg and a power density greater than 2 W/cm^3 relative to existing power converters for space application at 1 MHz. Fig. 5 outlines an efficiency vs. output current curve for this prototype board in comparison to the previous state of the art implementations of power converters. A minimum of 5% peak efficiency improvement was observed at output currents greater than 1A.

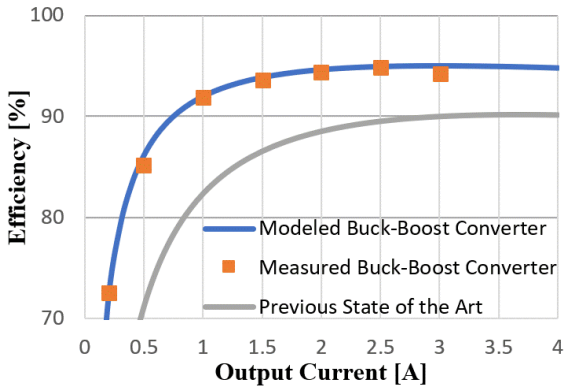

Figure 5: Measured efficiency vs. existing flight-qualified state of the art.

IV. SABER-RD SIMULATION OF BUCK BOOST CONVERTER W/ RCC

A simulation of the prototype synchronous buck boost converter was implemented in SaberRD (Synopsys). The RCC-based controller model was developed in SaberRD using the built-in StateAMS tool. To achieve accurate performance output in simulation, the utilized GaN transistor [17] was modelled in SaberRD using the power MOSFET tool. This tool uses the I-V and capacitance characteristics curve from the transistor manufacturers datasheet to create a precise model of the switch exhibiting real world performance in simulations [27].

Digital RCC Controller Design

The state diagram used to develop the RCC controller is shown in Fig. 6 below.

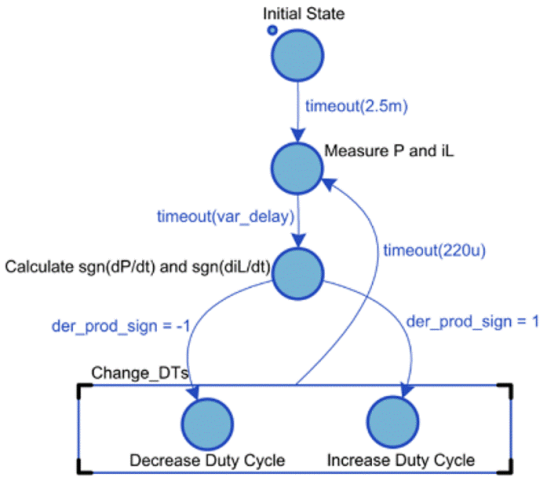

Figure 6: SaberRD StateAMS tool implementation of RCC. [28]

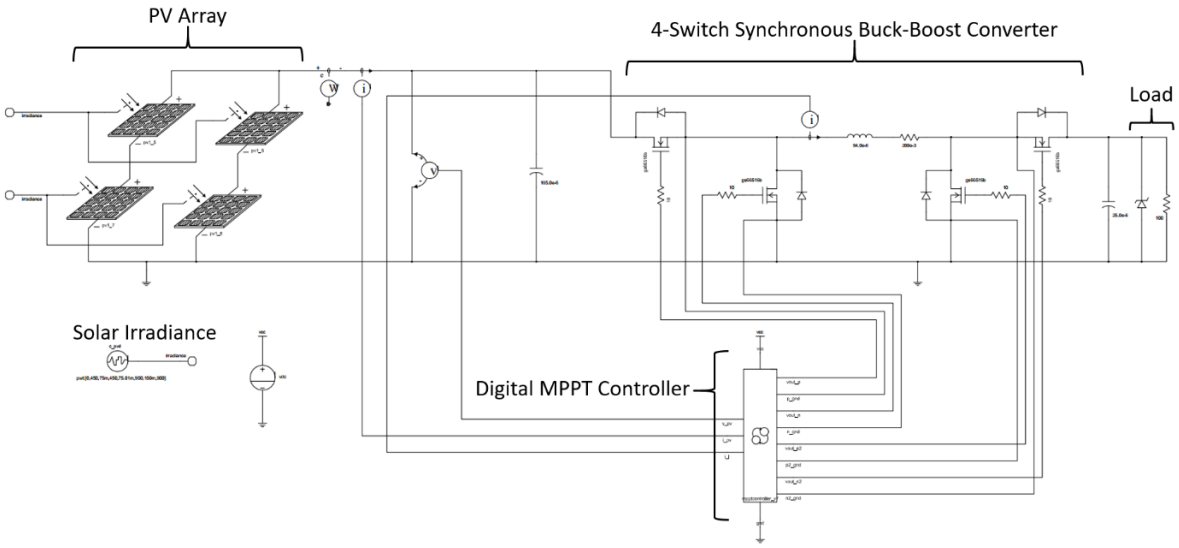

Figure 7: SaberRD simulation of synchronous buck-boost converter prototype with digital RCC-based MPPT controller. [28]

The StateAMS is a robust tool that can sample continuous signals as variables and apply mathematical operators, functions, or algorithms using state diagrams. In accordance with previous literature on RCC, the algorithm shown in Fig. 6 functions as follows: the system initially measures the PV voltage and current to calculate the PV power, and the inductor current of the converter. The system then utilizes the signum function (sign function) to calculate the sign of the time-based derivatives of both the PV power and inductor current. Next, the product of the signs of the aforementioned signals are taken. If this resulting product is positive, the algorithm increases the converter duty cycle, otherwise, decreases the duty cycle. This keeps repeating iteratively at regular time intervals and with the increase and decrease in the converter duty cycle, the voltage and current level of the PV array eventually converge to a steady level corresponding to the panel's MPP.

The duty cycle of the controller generated PWM signal depends on a continuous variable updating itself in the iterative loop shown in Fig. 6. Based on this variable, the PWM driving signal is produced with varying duty cycle to drive the high and low side transistors of the simulated synchronous buck-boost converter shown in Fig. 7. The digital controller also introduces a dead time into the PWM driving signal so that the switching of the high and low side transistors does not coincide.

Buck-boost Prototype Simulation

The SaberRD simulation schematic with the closed loop MPPT controller system, the buck-boost converter, and the input PV panels are shown in Fig. 7. The input of the converter was connected to a string of 4 PV panels oriented in a 2x2 series/parallel configuration. The panels each have an open-circuit voltage (V_{OC}) of 38V and a short circuit current (I_{SC}) of 1.8A at nominal temperature. The PV array V_{OC} is 76V, and I_{SC} is 3.8A corresponding to a solar insolation of 1000W/m^2. Fig. 8 shows the specifications for the panels at irradiance levels of 450W/m^2 and 900W/m^2. Fig. 8 (a) shows power versus current for the array, and Fig. 8 (b) shows power versus voltage. As can be seen from Fig. 8 (a), the maximum power for an irradiance of 450W/m^2 occurs at a current of approximately 1.5A, and a power of 100W. For an irradiance of 900W/m^2, the maximum power occurs at a current of approximately 3.2A and a power of 205W. These two operating points will be used to demonstrate the efficacy of the RCC-based MPPT controller developed in the StateAMS tool.

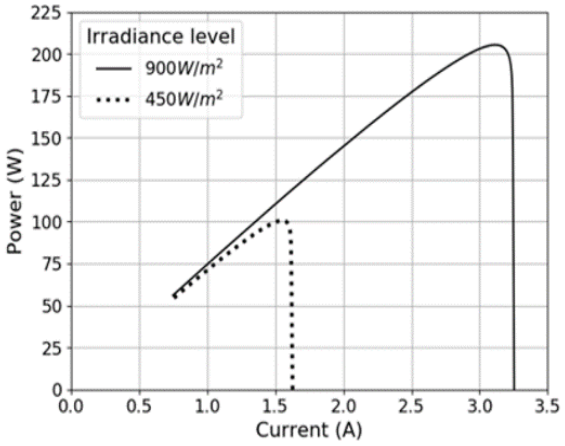

(a)

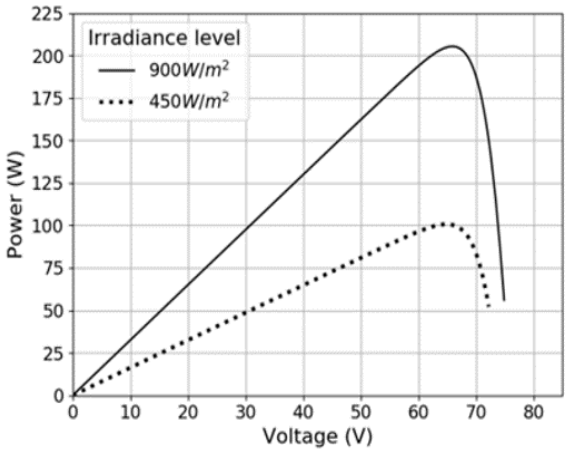

(b)

Figure 8: Simulated PV characteristics. (a) PV power vs. current. (b) PV power vs. voltage. [28]

The simulation switching frequency was set at 500 kHz, and the developed GaN transistor model was used. A 150ms simulation was performed. The simulation begins at an irradiance of 450W/m^2, and at 75ms, a simulated change in solar irradiance is injected into the system, forcing the irradiance to increase to 900W/m^2. Fig. 9 shows the irradiation versus time graph with the instant jump in irradiation level at 75ms.

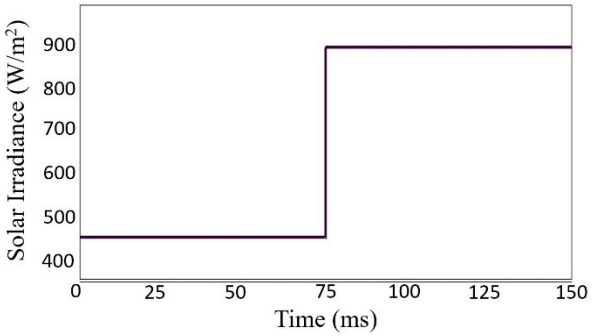

Figure 9: Change of solar irradiation at 75ms.

Simulation Results

The simulation results are illustrated in Fig. 10. The top waveform (orange) in Fig. 10 shows the PV output power versus time. After approximately 20ms, the output power settles at 100W, consistent with the MPP shown previously in Fig. 8 (a). Furthermore, as seen in Fig. 10, the power level changes exactly at 75ms, which is in alignment with the change in solar irradiation reflected in Fig. 9. In accordance with Fig. 8 (a) and (b), the rise in power level of the PV array is from 100W to 205W approximately. The middle waveform (red) in Fig. 10 shows the PV current level during the simulation time, which shows the shift in the output current at 75ms from approximately 1.5A to 3.2A, corresponding to the PV

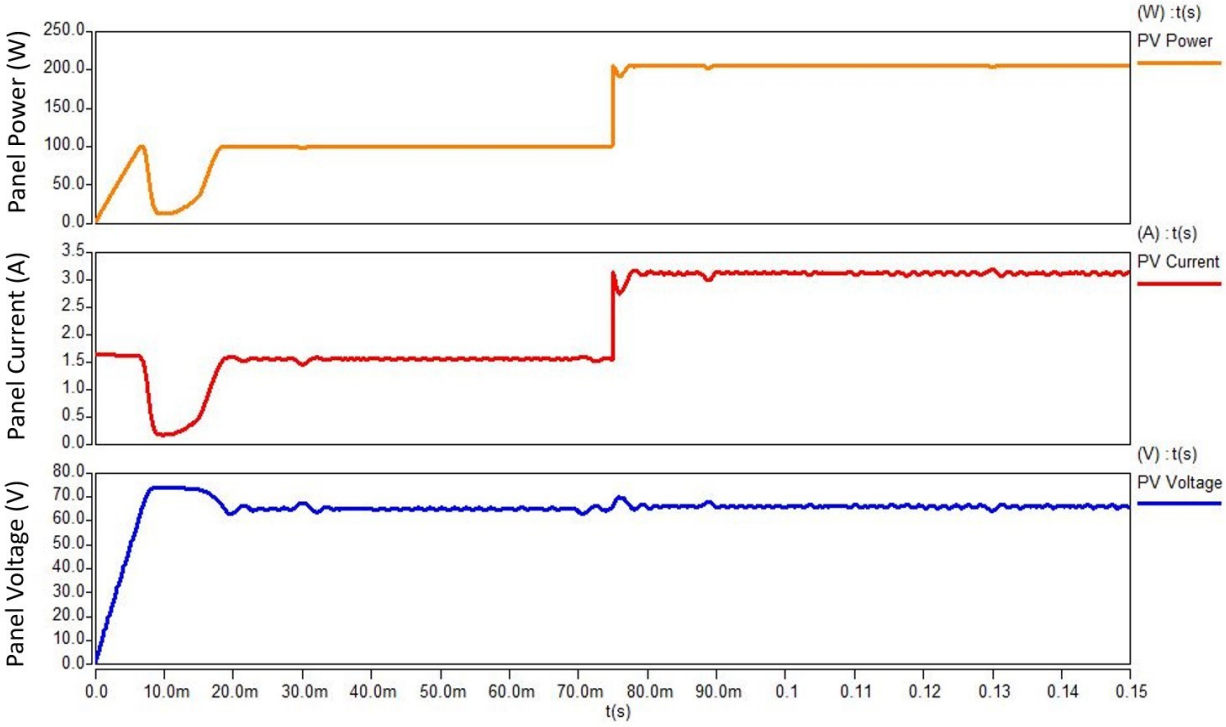

Figure 10: Output waveforms of digital RCC MPPT simulation. [28]

characteristic shown in Fig. 8 (a). The bottom waveform (blue) in Fig. 10 shows the PV array voltage settling approximately at 65V and remains at that voltage level throughout the simulation runtime corresponding to the PV characteristic shown in Fig. 8. It should be noted that from Fig. 8, it appears that the voltage at which maximum power occurs, for both 450W/m^2 and 900W/m^2 is approximately 65V.

The RCC principle as discussed in Section II is utilized by the digital controller, and is further demonstrated in Fig. 11, which shows the steady-state power and inductor current at around 43ms. As seen in Fig. 11 (a), at maximum power, the PV power and inductor current are in-phase with one another. Fig. 11 (b) shows the same two signals a few microseconds later where, the PV power and inductor current are out-of-phase, at maximum power. Although in Fig. 11 (b), the two signals have shifted slightly, the average maximum power is still obtained. This illustrates that the algorithm is iteratively utilizing the inductor current ripples to allow the PV power to oscillate about the maximum.

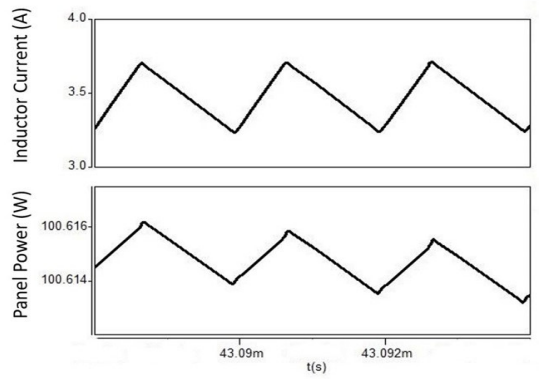

(a)

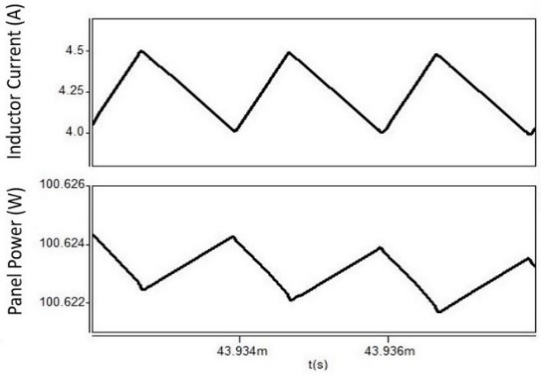

(b)

Figure 11: Time-domain simulations of pv power and inductor current. (a) the two signals in-phase. (b) the two signals out-of-phase. [26]

This section demonstrated the development of an RCC-based digital MPPT controller and the simulation results of the prototype synchronous buck-boost converter with this controller. From the outcome, it was clear that the controller swiftly and accurately tracked the MPP of the PV panel after the change of solar irradiation. The results also illustrated how the RCC does not require any external perturbation source and relies on the inherent PV power and inductor current perturbations caused by the converter switching activity.

V. CONCLUSION AND FUTURE WORK

This paper has shown that RCC is an excellent MPPT method to achieve accurate and rapid tracking in dynamic space environments. A synchronous buck-boost converter was proposed and prototyped to handle the wide voltage swings during a mission cycle. Due to the use of GaN transistors in the power converter, it was possible to push the converter to 500 kHz. Hence, a high power density could be attained which is a crucial factor to meet the design constraints for space applications. Also, a greater efficiency was obtained relative to the state-of-the-art implementations. The digital controller design demonstrated here was easily ported to a microcontroller to be used as the MPPT controller.

For future work, the digital RCC-based controller developed and used in the simulation will be validated experimentally using the prototype power converter board. In addition, the concept of model reference adaptive control (MRAC), as demonstrated in [29], will also be explored. By using MRAC the system will converge smoothly after a dynamic shift in solar irradiance. Furthermore, the adaptive moving average control proposed in [30] which is used to mitigate PV variability issues will also be explored.

References

1. C. Strümpel et al., "Modifying the solar spectrum to enhance silicon solar cell efficiency—An overview of available materials," Solar Energy Materials and Solar Cells, vol. 91, no. 4, pp. 238-249, 2007/02/15/ 2007.
2. M. O. Neill et al., "Advanced Development of Space Photovoltaic Concentrators Using Robust Lenses, Multi-Junction Cells, & Graphene Radiators," in 2018 IEEE 7th World Conference on Photovoltaic Energy Conversion (WCPEC) (A Joint Conference of 45th IEEE PVSC, 28th PVSEC & 34th EU PVSEC), 10-15 June 2018, pp. 3378-3383.
3. M. A. G. d. Brito, L. Galotto, L. P. Sampaio, G. d. A. e. Melo, and C. A. Canesin, "Evaluation of the Main MPPT Techniques for Photovoltaic

Applications," IEEE Transactions on Industrial Electronics, vol. 60, no. 3, pp. 1156-1167, 2013.

4. D. Selcan, G. Kirbis, and I. Kramberger, "Analog maximum power point tracking for spacecraft within a low earth orbit," IEEE Transactions on Aerospace and Electronic Systems, vol. 52, no. 1, pp. 368-378, 2016.
5. T. M. Lim, A. M. Cramer, J. E. Lumpp, and S. A. Rawashdeh, "A Modular Electrical Power System Architecture for Small Spacecraft," IEEE Transactions on Aerospace and Electronic Systems, vol. 54, no. 4, pp. 1832-1849, 2018.
6. O. Garcia et al., "Comparison of Boost-Based MPPT Topologies for Space Applications," IEEE Transactions on Aerospace and Electronic Systems, vol. 49, no. 2, pp. 1091-1107, 2013.
7. J. J. Soon, J. W. Chia, H. Aung, J. M. Lew, S. T. Goh, and K. Low, "A Photovoltaic Model Based Method to Monitor Solar Array Degradation On-Board a Microsatellite," IEEE Transactions on Aerospace and Electronic Systems, vol. 54, no. 5, pp. 2537-2546, 2018.
8. M. Rodríguez, Y. Zhang, and D. Maksimović, "High-Frequency PWM Buck Converters Using GaN-on-SiC HEMTs," IEEE Transactions on Power Electronics, vol. 29, no. 5, pp. 2462-2473, 2014.
9. W. Zhang, F. Wang, D. J. Costinett, L. M. Tolbert, and B. J. Blalock, "Investigation of Gallium Nitride Devices in High-Frequency LLC Resonant Converters," IEEE Transactions on Power Electronics, vol. 32, no. 1, pp. 571-583, 2017.
10. G. Sonia et al., "Proton and Heavy Ion Irradiation Effects on AlGaN/GaN HFET Devices," IEEE Transactions on Nuclear Science, vol. 53, no. 6, pp. 3661-3666, 2006.
11. T. Esram, J. W. Kimball, P. T. Krein, P. L. Chapman, and P. Midya, "Dynamic maximum power point tracking of photovoltaic arrays using ripple correlation control," IEEE Transactions on Power Electronics, vol. 21, no. 5, pp. 1282-1291, 2006.
12. A. M. Bazzi and P. T. Krein, "Ripple Correlation Control: An Extremum Seeking Control Perspective for Real-Time Optimization," IEEE Transactions on Power Electronics, vol. 29, no. 2, pp. 988-995, 2014.
13. A. Costabeber, M. Carraro, and M. Zigliotto, "Convergence Analysis and Tuning of a Sliding-Mode Ripple-Correlation MPPT," IEEE Transactions on Energy Conversion, vol. 30, no. 2, pp. 696-706, 2015.
14. J. W. Kimball and P. T. Krein, "Discrete-Time Ripple Correlation Control for Maximum Power Point Tracking," IEEE Transactions on Power Electronics, vol. 23, no. 5, pp. 2353-2362, 2008.
15. C. Barth and R. C. N. Pilawa-Podgurski, "Dithering Digital Ripple Correlation Control for Photovoltaic Maximum Power Point Tracking," IEEE Transactions on Power Electronics, vol. 30, no. 8, pp. 4548-4559, 2015.
16. M. Killi and S. Samanta, "Modified Perturb and Observe MPPT Algorithm for Drift Avoidance in Photovoltaic Systems," IEEE Transactions on Industrial Electronics, vol. 62, no. 9, pp. 5549-5559, 2015.
17. GaN Systems. "GS66516B." [Online]. Available: https://gansystems.com/gan-transistors/gs66516b
18. D. Kim and B. Lee, "An Enhanced Control Algorithm for Improving the Light-Load Efficiency of Noninverting Synchronous Buck–Boost Converters," IEEE Transactions on Power Electronics, vol. 31, no. 5, pp. 3395-3399, 2016.
19. M. Zerarka, P. Austin, A. Bensoussan, F. Morancho, and A. Durier, "TCAD Simulation of the Single Event Effects in Normally-OFF GaN Transistors After Heavy Ion Radiation," IEEE Transactions on Nuclear Science, vol. 64, no. 8, pp. 2242-2249, 2017.
20. L. Scheick, "Single-event effect report for EPC Series eGaN FETs: comparison of EPC1000 and EPC2000 series devices for destructive SEE," Jet Propulsion Laboratory, National Aeronautics and Space Administration, Pasadena, CA, 2014.
21. L. Scheick, "Status of the wide bandgap working group," NASA Electronic Parts and Packaging Program Electronic Technology Workgroup, Pasadena, CA, 2016.
22. O. Mourra, A. Fernandez, and F. Tonicello, "Buck Boost Regulator (B2R) for spacecraft Solar Array Power conversion," in 2010 Twenty-Fifth Annual IEEE Applied Power Electronics Conference and Exposition (APEC), 21-25 Feb. 2010 2010, pp. 1313-1319.
23. A. Barchowsky, A. Amirahmadi, C. Stell, E. Merida, G. Bolotin, and G. Carr, "A Class of GaN-Based, Radiation-Hardened Power Electronics for Jovian Environments," in European Space Power Conference, Juan-les-Pins, France, 2019.
24. A. J. Sellers, M. R. Hontz, R. Khanna, A. N. Lemmon, B. T. DeBoi, and A. Shahabi, "An Automated Model Tuning Procedure for Optimizing Prediction of Transient and Dispersive Behavior in Wide Bandgap Semiconductor

FETs," IEEE Transactions on Power Electronics, 2020, (in early access).

25. B. Sun, Z. Zhang, and M. A. E. Andersen, "A Comparison Review of the Resonant Gate Driver in the Silicon MOSFET and the GaN Transistor Application," IEEE Transactions on Industry Applications, vol. 55, no. 6, pp. 7776-7786, 2019.
26. K. J. Chen et al., "GaN-on-Si Power Technology: Devices and Applications," IEEE Transactions on Electron Devices, vol. 64, no. 3, pp. 779-795, 2017.
27. A. J. Sellers et al., "Effects of parasitic inductance on performance of 600-V GaN devices," in 2017 IEEE Electric Ship Technologies Symposium (ESTS), 14-17 Aug. 2017 2017, pp. 50-55.
28. S. Mahmud, "Development and Simulation of Maximum Power Point Tracking (MPPT) Controller with Ripple Correlation Control (RCC) for Deep Space Spacecraft," University of Toledo, OhioLINK Electronic Theses and Dissertations Center, 2020.
29. R. Khanna, Q. Zhang, W. E. Stanchina, G. F. Reed, and Z. Mao, "Maximum Power Point Tracking Using Model Reference Adaptive Control," IEEE Transactions on Power Electronics, vol. 29, no. 3, pp. 1490-1499, 2014.
30. R. Kini, D. Raker, T. Stuart, R. Ellingson, M. Heben, and R. Khanna, "Mitigation of PV Variability using Adaptive Moving Average Control," IEEE Transactions on Sustainable Energy, 2019, (in early access).